PHD TUTORIAL • **OPEN ACCESS**

How to determine the handedness of single molecules using Coulomb explosion imaging

To cite this article: Martin Pitzer 2017 *J. Phys. B: At. Mol. Opt. Phys.* **50** 153001

OPEN ACCESS
IOP Publishing
Journal of Physics B: Atomic, Molecular and Optical Physics
J. Phys. B: At. Mol. Opt. Phys. **50** (2017) 153001 (17pp)
https://doi.org/10.1088/1361-6455/aa77a9

Tutorial

How to determine the handedness of single molecules using Coulomb explosion imaging

Martin Pitzer

Experimental Physics IV, University of Kassel, Heinrich-Plett-Straße 40, D-34132 Kassel, Germany
Institute for Nuclear Physics, Goethe-University Frankfurt, Max-von-Laue-Straße 1, D-60438 Frankfurt, Germany

E-mail: martin.pitzer@uni-kassel.de

Received 12 May 2016, revised 2 May 2017
Accepted for publication 6 June 2017
Published 29 June 2017

Abstract

This tutorial is based on a doctoral thesis that was shortlisted for the 2016 AMOP dissertation prize of the German Physical Society (DPG). The principal achievement of the thesis was to use Coulomb explosion imaging (CEI) to determine the microscopic handedness ('chirality') of molecular structures on a single-molecule level. It thus shows how a technique developed in atomic physics can address a long-standing problem in chemistry. Owing to these disparate backgrounds, the tutorial has two facets: on the one hand, the history of molecular chirality and recent developments are very briefly reviewed. On the other hand, an account is given of different experimental approaches to CEI, on the physical processes in light-induced Coulomb explosion and—most importantly—on the aspects that are relevant when designing and performing such an experiment. As structural chirality occurs only in polyatomic molecules, special attention will be given to multiple ionization and multi-coincidence measurements. A short discussion of the results presented in earlier papers is given, followed by an outlook on experiments that are under way or can realistically be performed within the next years.

Keywords: chirality, coincidence measurement, stereochemistry, COLTRIMS, Coulomb explosion imaging, absolute configuration, photoionization

(Some figures may appear in colour only in the online journal)

This tutorial is structured as follows: the first three sections constitute an overview over the topic's various aspects, namely molecular chirality (section 1), development of detection and excitation techniques (section 2) and the physical processes that play a role (section 3) for the Coulomb explosion of chiral molecules. Section 4 depicts the experimental setup that was used to obtain the results presented in section 5, with both section trying to balance between general statements and an illustrative description. The last two sections provide an outlook on possible future developments (section 6) and a very short summary (section 7). As the tutorial covers a broad range of topics, only a few illustrative examples can be cited for each aspect. In most cases, the first reported results or a review are referenced so that the reader can hopefully get easily into further reading.

1. Introduction: molecular chirality

More than 150 years after its discovery, molecular chirality is still a vivid area of research and brings together physics, (bio)

chemistry and pharmacology. In the mid of the 19th century, Pasteur and others had discovered that many organic molecules form asymmetric crystals and that they rotate the polarization plane of light when they are in solution. As the concept of molecules was only developing during that period, the microscopic roots of this asymmetry remained unclear until 1874 when van't Hoff [1] and Le Bel [2] introduced—with similar reasoning but different concepts for the chemical bond—the concept of the asymmetric carbon atom. By this term, they designated a carbon atom that has four different substituents placed at the apices of a regular tetraeder. This configuration allows for two isomers (called enantiomers) that are mirror images of each other but cannot be brought into congruence by translation and rotation. As the two human hands show the same properties, Lord Kelvin derived the term 'chiral' for these molecules [3] from the Greek word for 'hand', and the notion of left-handed and right-handed molecules remains essential in the description of these isomers. Molecular chirality can be rooted not only in a chiral center (such as an asymmetric carbon atom), but also be due to a chirality axis, e.g. in the case of allenes, or the sense of helicity of a helical molecule, e.g. helicenes (for an overview over the stereochemic terminology, see [4]).

From the second half of the 19th century on, the field of stereochemistry rapidly evolved and the structural relations between many molecular species were revealed. A lot of ingenuity has been devoted since then to develop techniques that can distinguish between the two enantiomers. One has to keep in mind that pure samples of left-handed and right-handed molecules respectively do not show any measurable difference in scalar properties (thermodynamic properties, energy levels, nuclear magnetic resonance signals etc). In order to get distinct signals from the enantiomers, one can utilize other chiral molecules (chromatographic approaches) or light of a well-defined polarization state (chiroptical approaches). Well-known examples for the latter are optical activity (rotation of the polarization plane), circular dichroism (different absorbance of left- and right circularly polarized light) and optical rotatory dispersion (wavelength dependent measurement of the optical activity). Another trick for analysis is to have the chiral molecules react with a second chiral species to form diastereomers. Like enantiomers, diastereomers are isomers that only differ by the spatial direction of bonds but contrary to the former, they are not mirror images of each other; a well-known example is *cis*/*trans* isomerism (for details see [4]). Diastereomers of a chemical species show different physical and chemical properties so that they can be distinguished by a wealth of techniques. An overview over analytic methods can be found in [5], a more detailed description of various chiroptical approaches in [6].

For a long time, however, it had been impossible to directly determine the microscopic handedness of the molecular structure. All techniques mentioned above need additional input, either from theoretical models or from relations with species for which the microscopic configuration is known. As long as no reference structure was available, only relative but no absolute configurations could be determined. In 1891, Emil Fischer had arbitrarily assigned one of the two possible microscopic structures to the dextrorotatory saccharic acid [7], but this commonly used designation could not be verified for decades.

In 1951, Bijvoet and co-workers used anomalous x-ray diffraction to determine the absolute configuration of sodium rubidium tartrate [8]. At that time, x-ray diffraction of crystallized samples had become a powerful tool for structure analysis of organic molecules. In elastic scattering, however, the diffraction pattern only depends on phase differences of the scattered waves so that the spatially inverted enantiomers cannot be distinguished. Anomalous x-ray diffraction, on the contrary, makes use of an additional phase shift that occurs for resonant scattering, leading to different patterns for the two enantiomers. That work confirmed that Fischer's choice had by chance been correct. Around the same time, Cahn, Ingold and Prelog developed a systematic nomenclature for assigning the labels *R* (from Latin *rectus*) and *S* (from Latin *sinister*) to the structure models [9, 10].

In the last two decades, several gas-phase techniques have been applied to investigate chiral molecules and to discriminate between enantiomers; among them are angle-resolved photoelectron spectroscopy (photoelectron circular dichroism (PECD) [11–13]), laser-induced mass spectroscopy [14, 15] and microwave three-wave mixing [16]. In addition, Coulomb explosion imaging (CEI) has been shown to yield the microscopic configuration of simple chiral molecules [17–20]. The remainder of this tutorial will be devoted to describing the development and an implementation of CEI and to outlining its future potential in the context of chiral molecules.

2. A brief history of CEI

The basic idea of CEI is quite simple: remove so many electrons that the repulsive forces of the atomic cores outweigh their mutual binding. The strong repulsion will then cause the ionic cores to 'explode' until they do not experience any interaction anymore. The *axial recoil approximation* assumes that the momentum directions of the fragments correspond to the bond axis in the molecule. This approximation works best for diatomics; the more complex the molecule is, the more deviations from this relation are expected. It is also obvious that the axial recoil approximation can only hold if the fragmentation occurs on timescales smaller than vibrational and rotational periods of the molecule.

The transformation from initial positions into the momenta of fragments can also be understood in an energy surface picture: upon electron removal, repulsive potential surfaces are populated; the system then evolves on these surfaces until it reaches the asymptotic region. The energy difference between the level populated in the excitation step and the asymptotic value is transformed into kinetic energy of the fragments. It should be clear at this point that CEI exclusively deals with positive ions (cations); in the remainder of the article, the term 'ions' always refers to cations unless otherwise stated.

Determination of the structural features by using the axial recoil approximation requires ionization and fragmentation to be fast compared to the timescale of nuclear dynamics. Consequently, two requirements are essential for any implementation of CEI: firstly, a sufficient number of electrons must be removed within a time-scale shorter than structural distortions; secondly, the relative directions (i.e. the momentum vectors) of the fragments must be recorded 'simultaneously' or more precisely: in coincidence. For a long time, however, it was impossible to fulfill these prerequisites. Whereas fast multiple ionization could in principle be induced with techniques available in the 1950s and 1960s (see section 3.1), detector technology and computers for analysis were only from the late 1970s sufficiently developed to record and treat the data that are necessary to reconstruct several fragments' momentum vectors.

At that time, the first successful attempts to investigate molecular structure by dissociation came from high-energy physics where the study of fragmentation processes and the corresponding experimental techniques had been developed for decades. Using electrostatic accelerators, molecular ions could be brought to kinetic energies of several MeV, corresponding to a velocity of a few percent of the speed of light. When such a molecular beam traverses a foil with a thickness of 10 nm or less, electrons are stripped off within less than a femtosecond. The atomic ions repel each other, leading to small deviations in their trajectory. These deviations can be measured by detectors downstream, allowing to determine the dissociation energies. Mass separation of the fragments can be achieved by magnetic fields between interaction region and detectors. First experiments were reported on simple ions like HeH^+ [21]. Using different kinds of multiparticle detectors [22, 23], the configuration of the CH_4^+ ion [24, 25] as well as the structure of small carbon clusters [26, 27] and the bond angle distribution of H_2O^+ [28] were investigated. Although the swiftness of electron removal is still unsurpassed, foil-induced Coulomb explosion has several drawbacks: in the first place, molecular ions have to be created and it has to be taken into consideration that the structure (and possibly even the configuration) can be different from the neutral molecule. Secondly, the passage through the foil needs to be fast enough, implying an upper boundary for the molecular mass; the maximum mass depends on the energy of the accelerator but rarely exceeds 100 atomic mass units. Finally, the physical size of the experiment and the expertise in running the accelerator require resources that are not commonly available.

In parallel to foil-induced Coulomb explosion, coincident ion imaging setups had been developed for reactions in crossed ion-neutral beams [29] and the photodissociation of small neutral molecules [30]. In the latter case, the duration of the exciting laser pulse (picoseconds to nanoseconds) could reveal photodissociation processes but not the initial structure.

In the 1990s, first experiments on the Coulomb explosion of neutral species were reported. Most of the respective techniques can be considered as an extension of time-of-flight (TOF) mass spectrometry in the sense that mass-selectivity and differentiation of momenta are achieved by an electrostatic spectrometer. An early three-dimensional momentum imaging setup was used to investigate complete fragmentation of water molecules [31] induced by H^+ and He^+ beams; the time- and position-sensitive coincident detection was performed by a combination of a microchannel plate (MCP) and an anode implemented as a two-dimensional array of wires [32]. The bond angle distribution calculated from the data was in relatively good agreement with theoretical values. A drawback of this approach was the large number of signal channels employed (16 for each dimension of the detector).

A helical delay line as position sensitive anode [33], in contrast, uses only two signal channels per dimension as the position information is encoded in the run-time difference (for details see section 4.5). Using this detection method [34] together with photoionization by gas discharge lamps ($h\nu = 48.4$ eV), fragmentation of OCS, SO_2, CS_2, N_2O and ICN into two ions and a neutral atom were investigated. A detailed account of fragment energies and angles between the momenta is given in [35].

The development of femtosecond lasers enabled an additional way to induce the instantaneous multiple ionization of molecules. In the first years, the low repetition rate prevented coincident detection (see section 4.1). As a consequence, covariance analysis [36] was often used to obtain fragment energies after Coulomb explosion, e.g. for C_2H_2 [37]. As the name suggests, this method uses statistics to extract information on the molecule from fragment correlations. Another widespread approach are 2D imaging techniques, most prominently velocity map imaging [38]. As these techniques do usually not measure ions in coincidence, the abundant literature using these techniques will not be reviewed here. A particular appealing feature of laser experiments is the possibility for pump–probe schemes. In this case, the molecule is first excited by a weaker pump pulse; structural changes can then be imaged by Coulomb explosion induced by the probe pulse. An early example for imaging the time-dependent structure of a dissociating molecule (I_2) is [39]. The first experiment using triple coincidences is to the author's knowledge a study of SO_2 that followed the breaking of the two bonds in time [40].

After the year 2000, CEI and coincidence techniques found widespread application in the atomic physics community. One of the reasons was the development of the 'reaction microscope' or cold target recoil ion momentum spectroscopy (COLTRIMS) technique [41, 42], that allows one to measure momenta of ions and electrons on two separate detectors. This makes it possible to study electron distributions in the molecular frame defined by the ions' momentum vectors (e.g. [43, 44]). The majority of experiments are, however, restricted to the detection of two ionic fragments in coincidence.

Purely ion imaging setups were at the same time used to reveal structural features of larger molecules. Kitamura *et al* used Ar^{8+} at an energy of 120 keV to investigate the 'dynamic' chirality of perdeuterated methane (CD_4), i.e. the different bond lengths that occur at any instant due to

vibrational motion [45]. One of the few examples for five-fold coincidences is a study of CH_2Cl_2 after laser excitation [46]. Various relations between the fragment velocities were explored and a reconstruction of the molecular structure was performed in that work. An example for CEI of larger molecules is benzene, investigated using laser ionization [47] and ion collisions [48].

In recent years, ionization to extremely high charge states and pump–probe experiments with extreme UV and x-ray radiation have become possible by using free-electron lasers (FELs, see also section 3.1). In parallel, established techniques such as electron impact continue to provide insights on the structural information from coincident momentum imaging of three-particle break-ups of polyatomic species such as CO_2 [49] or H_2O [50].

The determination of the absolute configuration of chiral molecules is an example of how CEI can be applied to a question of fundamental importance in chemistry. This step was achieved independently by laser-induced CEI using the COLTRIMS-technique [17] and foil-induced CEI [19, 20]. In the former experiment, a racemate of the chiral prototype CHBrClF was fully fragmented, allowing the assignment of handedness for individual molecules. In the latter case, an enantiopure sample of 2,3-dideutoro-oxirane ($C_2H_2D_2O$) allowed to directly relate microscopic and macroscopic nomenclature and to confirm Emil Fischer's choice [51]. Another recent imaging experiment on a halogenated biphenyl used adiabatic alignment of the molecules by a preceding nanosecond pulse. Covariance analysis of two fragments allowed to determine the absolute configuration of isolated molecules even without coincident detection of fragments [52].

3. Multiple ionization and fragmentation of molecules by photons

In order to achieve multiple ionization and fragmentation, a sufficient amount of energy must be deposited in the molecular system. If we follow Einstein in his explanation of the photoelectric effect, this means that photons with a small wavelength are needed; in the case of four- or five-fold ionization necessary for multiple fragmentation, photons must be in the soft x-ray region. This is, however, not a necessary condition in the non-linear optical regime. If the intensity (i.e. the photon density) of the light is sufficiently high, the energy can be acquired by absorption of several photons—up to the high-intensity limit where the number of photons is so large that the classical field description gets back its validity.

Following these interaction regimes, this section is divided into two parts: the first one will sketch the essentials of multiple ionization with a single photon. In the second part, a glimpse into the description of strong-field ionization will be given. The discussion here will be restricted to the physical processes; how these are experimentally implemented in CEI experiments will be described in section 4.2.

3.1. Single-photon ionization

In the case of single-photon ionization, the light–matter interaction is usually described by quantum mechanical perturbation theory: the transition probability $W_{i\rightarrow f}$ from the initial state $|\Psi_i\rangle$ to the final state $|\Psi_f\rangle$ is given by Fermi's Golden Rule

$$W_{i\rightarrow f} = \frac{2\pi}{\hbar}|M_{if}|^2\delta(E_f - E_i - \hbar\omega), \quad (1)$$

where the transition matrix element M_{if} is usually given in the electric dipole approximation. A more detailed description can be found in most advanced quantum mechanics textbooks, e.g. [53].

As can be seen in equation (1), the probability for this process essentially depends on the matrix element. Using a concept from scattering physics, the transition probability is usually expressed as a cross section σ, representing the 'effective' area of the atom or molecule for photon impact. Together with the photon flux and the density of target molecules, the cross section allows one to estimate the rate of excitation and is an important parameter in the design of an experiment. If the photon energy is higher than the binding energy of an electronic state, the absorption of one photon leads to direct emission of one photoelectron. Detailed tables on the photoionization cross sections are available (e.g. [54]). If the photon energy is a few electron volts lower than the binding energy, resonant excitation into unoccupied states of the molecule can occur. The cross section for these resonant processes can be higher than for direct photoionization; additionally, state selection of the excited state can be achieved in this case.

For Coulomb explosion to occur, multiple ionization is mandatory. It has been mentioned that photons in the soft x-ray region are necessary from an energy point of view. Which processes lead then to the emission of several electrons? The most prominent one is expected to be Auger decay. In this case, the electronic configuration of the atom or molecule relaxes by emitting additional electrons. More pictorially speaking, the hole created by the absorption of a photon is filled by an electron from an energetically higher level; the excess energy is transferred to another electron that can thus leave the atom or molecule. Auger decay can occur as well for resonant excitation as for photoionization. High probabilities for four- and five-fold ionization of rare gas atoms upon irradiation with x-ray tubes have already been demonstrated in the 1960s [55]. Tunable x-ray radiation from synchrotron sources and photoelectron-photoion coincidence spectroscopy, as well as detailed calculations, have deepened the understanding of these processes in recent years [56, 57]. In addition to Auger decay, direct double photoemission of electron pairs (shake-off or knock-off/two-step-one processes) can contribute as well to multiple ionization [58]. The latter can be understood as an (e, 2e)-collision caused by the outgoing photoelectron. An additional process with a very small cross section is the direct emission of two photoelectrons by absorption of one photon, creating so-called double core-hole states (see e.g. [59]).

The electronic processes after core excitation usually occur on the timescale of attoseconds or a few femtoseconds, i.e. much faster than most structural distortions of the molecule. It has, however, been shown that fragment dynamics can occur on the same time scale as electronic processes (ultrafast dissociation [60]). In addition, intermediate molecular states could be produced that undergo structural deformation before further dissociation (e.g. [61]). In the case of an 'equal' distribution of charges between atomic sites that is necessary for Coulomb explosion pathways, the electronic decays are expected to happen before significant nuclear rearrangement takes place (which can in part be justified *a posteriori* from the measured momenta). Due to the multitude of possible processes in polyatomic molecules, the interplay of charge rearrangement and nuclear dynamics is an active research field, having gained new impetus by the possibility of x-ray pump–probe schemes with free electrons lasers [62].

Even for a fixed photon energy, the multitude of processes in the ionization and charge rearrangement leads to a variety of fragmentation pathways of which only a few yield information on the absolute configuration of chiral molecules. Increasing the yield of relevant channels by identifying a promising selective excitation scheme might thus be beneficial [63, 64].

3.2. Multi-photon and strong-field ionization

With the light intensities provided by lasers, non-linear optics can be realized, i.e. processes where two or more photons are absorbed 'simultaneously'. In the case of atoms and molecules, ionization can take place at photon energies much below the ionization threshold. The effects of multi-photon ionization have been studied for decades. In most cases, however, the ionization state obtained is not sufficiently high to induce multiple fragmentation.

If the intensity of the light surpasses 10^{14} W cm^{-2}, the electric field reaches values comparable to the Coulomb field that the electrons experience from the atomic nucleus. This oscillating superposition converts the potential well of the nucleus to a barrier through which bound electrons can tunnel. A well-known description of this process is the semi-classical ADK model [65] that has also been extended to molecules [66–68]. A more rigorous quantum mechanical treatment is provided by the strong-field approximation, pioneered by Keldysh, Faisal and Reiss [69–71]. A description providing a reasonable mixture of intuitive explanation and theoretical background is given in [72], a more thorough theoretical review can be found in [73]. This model has successfully been applied to diatomic [74] and polyatomic [67] molecules.

Multiple ejection of electrons from a molecule in a strong laser field can occur either independently ('sequentially') or involving electron–electron correlation. These correlation effects are expected to dominate and have extensively been investigated in the last two decades, especially the non-sequential double ionization of different atomic and molecular species (for a review see e.g. [75]). A very prominent process for double ionization is the so-called recollision where an emitted electron acts back onto the atom or molecule and ejects a second electron [76], an effect that has also been investigated for polyatomic molecules, e.g. [77]. Another mechanism expected to be important for multiple ionization of molecules is the charge-resonance-enhanced ionization [78, 79], leading to an enhanced ionization probability when the cores have already started dissociating. For more complex molecules and higher ionization states, only a few systematic experimental studies are available [77, 80] and current theoretical models reach their limit at higher numbers of emitted electrons.

As in the case of single-photon ionization, the variety of effects leads to a multitude of fragmentation pathways at given experimental conditions. An additional experimental complication in the case of strong-field ionization is the spatial variation of intensity in the laser pulse. Although a more detailed understanding of the ionization mechanism will help to reach the relevant ionization states with higher probability and better selectivity, experience has shown that this knowledge is not mandatory to perform a Coulomb explosion experiment.

4. Technical aspects of a CEI experiment

Several examples of CEI have been discussed in section 2. The following section describes the experimental details of a specific implementation: the use of a COLTRIMS/reaction microscope setup [41, 42], essentially composed of a molecular jet, an electrostatic spectrometer, time- and position-sensitive single-particle detectors and the corresponding data acquisition and analysis tools.

The following description is restricted to a pure ion imaging setup; in many COLTRIMS applications, electrons are measured as well. Their detection requires additional features at several stages. In addition to a general overview of the experimental technique, the peculiarities of measuring a larger number of ions ($n \geqslant 4$), are discussed. This section of the tutorial thus is not only valid for the investigation of chiral molecules. Section 5 will illustrate these rather abstract considerations via the example of the chiral prototype CHBrClF. Discussing the procedures in detail, however, is beyond the scope of this tutorial. More detailed information can be found in [81], but also in various doctoral theses dealing with the COLTRIMS technique.

Previous to the various experimental components, a short section will present the principles of 'event-based' measurements as they might be less familiar to many readers from the molecular physics and physical chemistry community.

4.1. Particularities of event-based measurements

The key point of a Coulomb explosion or any other coincidence experiment is the fact that one molecular fragmentation after the other is recorded; any property or feature in a spectrum will only become visible by integrating over a sufficient number of these 'events'. Otherwise, features will be hidden by the statistical uncertainty which in many other

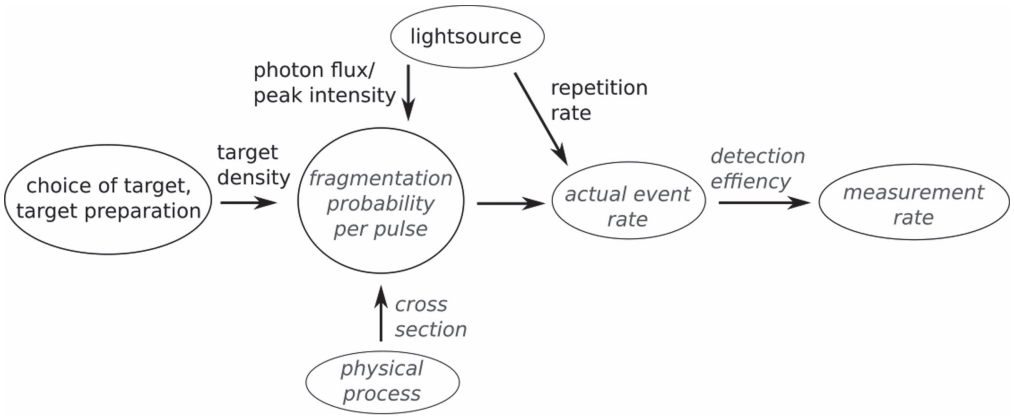

Figure 1. Parameters that influence the measurement rate in a coincidence experiment. The factors written in normal font depend only on the experimental implementation and are identical for the different break-up channels of a molecule. The factors in italic font may vary for different break-ups of the same molecular species. For a more detailed discussion, see text.

contexts is a factor contributing to the 'signal-to-noise' ratio. As a consequence of this event-counting, all data are displayed in histograms, i.e. the signal strength is given in 'counts' (=number of events). During measurements, a key parameter is the rate (events per second) at which these events take place.

Figure 1 is an attempt to visualize the interplay of factors that will be mentioned in the following subsections. The diagram should be read from right to left: let us first assume, for simplicity, that the molecule under investigation has only one possible fragmentation pathway. The rate with which this fragmentation is recorded by the detector is lower than the actual rate because the detection efficiency is significantly below 100% (see section 4.5); this problem aggravates with the number of ions to be detected in coincidence because the detection efficiencies of the particles are multiplied.

The actual event rate depends on the repetition rate of the light source and on the probability that the ionization and subsequent fragmentation process is triggered by a light pulse. The fragmentation probability itself is a product of three factors: first the cross section of the physical process that leads to fragmentation, second the properties of the light pulse (number of photons in the single-photon case or light intensity in the strong-field case), and third the density of target molecules in the interaction region. The first two aspects will be discussed in section 4.2, the last one in section 4.3. It must be remembered at this point that the coincident detection of the fragments requires a single-molecule condition: each light pulse should fragment one molecule at most; to keep the probability of fragmenting a second molecule below 10%, the ionization probability per pulse should less than 10% as well (assuming Poisson statistics). Practically, this probability is determined by the ratio between the repetition rate and the count rate; given that not all fragmentation events are recorded due to the limited detection efficiency, the ratio between measured rate and repetition rate of the light source should ideally be lower than $1/10$. This means that the parameters have to be tuned in a way that on one hand, this condition still holds, and on the other hand the measurement rate is maximized. It should be remembered that increasing the pulse energy (in the laser case) or the photon flux per pulse (in the synchrotron case) by a factor X is not equivalent to increasing the repetition rate by the same factor.

This scheme is complicated by the fact that—against our first simplistic assumption—not only one distinct fragmentation pathway occurs for a given excitation of the molecule. The parameters in italic font in figure 1 are specific for each fragmentation: the cross section for the fragmentation obviously depends on the exact physical process, so that different fragmentations occur with different event rates. It is less obvious that also the detection efficiency depends on the fragmentation pathways, e.g. that it is lower for break-ups with more particles.

Especially for multiple coincidences ($n \geqslant 4$), the ratio of detected relevant fragmentations compared to the total count rate is very low. For the experiments reported below, it was between a few times 10^{-6} and several 10^{-4}. This makes it necessary to play with the different experimental parameters to obtain a reasonable yield for such low-probability break-ups and to simultaneously fulfill the coincidence condition for more abundant channels.

4.2. Photon sources

As mentioned in section 3, two types of light sources—corresponding to two different ionization mechanisms—can be used for the multifragmentation of molecules. Having discussed the respective ionization mechanisms and a few examples for CEI in the previous sections of this tutorial, this part is restricted to technical considerations.

4.2.1. Femtosecond lasers. In the last 20 years, femtosecond lasers have revolutionized optical spectroscopy in many areas. Nowadays, most of the systems used in molecular physics rely on chirped pulse amplification in titanium-doped sapphire (Ti:sapphire) crystals, centered at a wavelength of around 780 nm. Detailed descriptions can be found in many textbooks, e.g. [82], and systems are available commercially. To use them for Coulomb explosion experiments is nevertheless still

challenging: on the one hand, the intensity, i.e. the energy per pulse, must be high enough to induce multiple ionization; for the results presented below, 40 fs pulses with an energy of 10 μJ ($P_{\mathrm{peak}} = 100$ MW) were focused by a silver mirror ($f = 60$ mm) to reach intensities of 6×10^{14} W cm^{-2}. On the other hand, the repetition rate must be high enough to allow for a reasonable rate of break-ups, as discussed in the previous section. The results presented below were obtained using a KMLabs Wyvern500 regenerative amplifier running at a repetition rate of 100 kHz. At the intensities required for multiple ionization, the probability for single ionization of a molecule in the laser focus goes close to one. This means that the number of target molecules (the target density) must be so low that the coincidence condition holds (see section 4.3).

A major drawback of the femtosecond laser approach is the fact that the ionization of molecules in the strong-field regime depends mainly on the ionization potential of the highest occupied orbitals (e.g. [66]). As a consequence, the ratio between relevant fragmentation pathways and total ionization events is hardly tunable—at a given repetition rate, an increase in laser intensity to achieve a reasonable rate of multiple fragmentation will lead to an overwhelming amount of single and double ionization events. Thanks to advances in various technologies—especially Ti:sapphire amplifiers [83], fiber lasers [84, 85], optical parametric amplification schemes [86] and high-power thin-disk oscillators [87]—femtosecond lasers with the required peak power of roughly 100 MW and repetition rates in the MHz range will likely be available in the near future, allowing to measure at higher count rates and thus tackle this problem.

Another disadvantage, especially when protons are to be detected, is the duration of the laser pulse which is of the same order as the CH stretching mode. This leads to a broadening in the measured proton distribution. As several laser cycles seem to enhance the probability for multiple ionization, it is still unclear to what extent shorter pulses will remedy this problem. The use of extreme UV or soft-x-ray pulses from high-harmonic generation to fragment molecules has been pioneered a decade ago [88] and meanwhile been extended to polyatomic molecules [89]. This opens the possibility to perform single-photon induced CEI with a table-top setup and allows pump–probe experiments with combinations of IR and UV pulses.

4.2.2. Synchrotron radiation sources. As described in section 3.1, multiple ionization of molecules can also be induced by single x-ray photons. Photons in the appropriate energy range are provided by synchrotron radiation sources. In these large-scale facilities, bunches of electrons circulate in a storage ring at relativistic energy; in so-called 'insertion devices' (nowadays mostly undulators), they are subject to alternating magnetic fields, leading to emission of light with high flux and small divergence. Monochromators in the beamline can select a certain energy with high resolution ($E/\Delta E \approx 50\,000$). Although the duration of the light pulses can be hundreds of picoseconds, the single photon absorption occurs quasi instantaneously compared to nuclear time scales.

In the case of single photon ionization, the ionization rate r is usually estimated by $r = \sigma \cdot \Phi \cdot n$ where σ is the ionization cross section (in m^2), Φ is the photon flux (in s^{-1}) and n is the target density, i.e. the density of molecules multiplied by the thickness of the target seen by the photon beam (in m^{-2}).

The results described below have been obtained in the timing mode of the synchrotron. In this operation mode, only one or a few bunches circulate in the storage ring, leading to pulses with a separation of a few hundred nanoseconds, i.e. to repetition rates of several MHz. This mode is mandatory for experiments with electron-ion coincidences because the electrons need to arrive at the detector in the time between two bunches; otherwise, it is impossible to determine which light pulse induced the ionization, and thus impossible to determine the TOF of the fragments. For pure CEI, the electron TOF information is not needed, so that the arrival of the electron on a detector can be used as starting clock for the TOF measurement of the ions, as in early ion coincidence experiments [90, 91]. Several fixed setups exist at synchrotrons that are in principle capable of performing CEI [92, 93]. Alternatively, a user setup can be attached to beamlines that have no fixed endstation.

FELs can provide x-ray pulses with duration in the femtosecond range. Due to the high photon flux, the amount of residual gas and the target density have to be extremely low to enable coincidence conditions; the low target density can, however, be an advantage since it enables measurements with very small amounts of sample and low vapor pressures. A drawback for Coulomb explosion is the rather low repetition rate of currently existing FELs.

4.3. Target preparation

In order to perform CEI, the molecules under investigation must be brought in the gas phase into an ultra-high vacuum chamber. In most cases, the target is provided by a supersonic or effusive jet: from a reservoir with high pressure, the sample is expanded into the vacuum; the jet is usually skimmed by one or two small apertures to maintain a low background pressure in the interaction chamber. We have seen in section 4.2 that for a given photon source, restrictions may apply to the target density. While for femtosecond lasers, a low target density is rarely a problem, synchrotron experiments are usually not feasible a stagnation pressure below 100 mbar.

For this reason mostly substances with high vapor pressure have been investigated by CEI. Heating the sample in an 'oven'—as well as the nozzle—is the easiest way to increase the vapor pressure, but is only feasible for substances that do not decompose (or change their structure) at increased temperatures. Various sample preparation schemes such as laser desorption (e.g. [94]) and thermodesorption of preformed aerosols (e.g. [95]) have successfully been applied in mass-spectroscopic studies with synchrotrons and femtosecond lasers and can in principle be used for CEI. In some cases,

e.g. to form a supersonic jet with a small amount of sample or for species that easily form dimers such as acids, pick-up of the sample with an inert gas (preferably helium due its small ionization probability) can be beneficial.

The role of cooling by the supersonic expansion is still unclear. Fragments gain energies of several electron volts so that the thermal translational energy of 25 meV at room temperature can be neglected. Thermal excitation of rotational and vibrational degrees of freedom can, however, broaden the initial spatial distribution of the nuclei and consequently of the momenta, so that determination of configuration might be more straightforward for cold molecules. For larger molecules it is difficult to estimate the actual temperature in the jet due to their many degrees of freedom. Semi-empirical rules and parameters also for polyatomic molecules can be found in [96]. Freezing the internal degrees of freedom is expected to be more relevant in the case of single-photon excitation; for strong-field excitation, the dynamics in the laser field are probably dominant in broadening the momentum distribution.

What has been important both for synchrotron and laser ionization, is the spatial confinement due to the jet: when molecular jet and photon beam are crossed at right angle, the interaction volume is well characterized, so that no focusing spectrometer design is necessary (see section 4.4). In the case of ionization by laser pulses, the Rayleigh length of the focus can be decreased to a few hundred μm by a small focal length, so that experiments might be possible where the sample is not provided as a well-defined jet. The single ionization that occurs even from the unfocused beam might however contaminate the Coulomb explosion data severely.

4.4. Spectrometer

The spectrometer is the part of the experiment that is separating the fragments according to their masses and momenta and guiding them to the detector. Like in a common TOF mass spectrometer, an electrostatic field accelerates the ions and leads to arrival times at the detector that depend on the mass-to-charge ratio m/q. Purely mass-analyzing setups employ a field design that compensates for the initial velocity distribution of the fragments and focuses the ions onto a small detector to achieve good mass resolution and a high signal strength at comparatively low cost. In a 'standard' COLTRIMS setup for CEI, by contrast, only a homogeneous electric field with a modest field strength (a few up to 100 V cm^{-1}) is used. In such a field, the velocity component along the spectrometer axis affects the TOF in a measurable amount: ions ejected towards the detector arrive at earlier times than those ejected in the opposite direction. Perpendicular to the spectrometer axis, the ions propagate with their initial velocity until they reach the time- and position-sensitive detector (see next section). Figure 2 illustrates this principle for a diatomic molecule. Simulations show that it is a good approximation for the analysis to separate the acceleration of the ions in the Coulomb explosion from the motion in the electric field of the spectrometer, due to the fast timescale and small spatial extent of the Coulomb interaction. The momenta gained in the explosion can thus be retrieved by

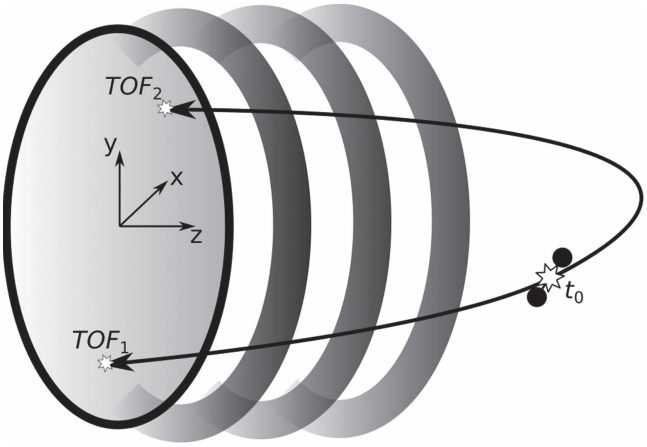

Figure 2. Sketch of a spectrometer for momentum imaging. The molecule—for illustration purposes a diatomic—is ionized at time t_0. The positively charged atoms repel each other and gain momentum predominantly along the initial bond direction. The electric field induced by the spectrometer plates (gray rings, cut for better visibility) guides the ions to a time- and position-sensitive detector. For a given mass, the time-of-flight (TOF) together with the impact position allows one the initial momenta (equation (2)).

assuming classical trajectories in the spectrometer. For a homogeneous electric field along the spectrometer (z-axis) and field-free propagation along the x- and y-axis, the relations read

$$p_x = \frac{x \cdot m}{\mathrm{TOF}}, \tag{2a}$$

$$p_y = \frac{y \cdot m}{\mathrm{TOF}}, \tag{2b}$$

$$p_z = -\frac{1}{2} q \cdot E \cdot \mathrm{TOF} + \frac{m \cdot s_{\mathrm{acc}}}{\mathrm{TOF}}. \tag{2c}$$

The dimensions of the spectrometer and—once this is fixed—the electric field should be chosen according to the properties of the Coulomb explosion and the fragments to be detected. A low electric field will, on the one hand, lead to a wide spread in the TOF and thus to better momentum resolution in the spectrometer direction. On the other hand, the longer TOF will increase the spread along the perpendicular axes as well, up to a point where not all fragments can be guided onto the detector. A compromise has thus to be found that yields good momentum resolution and still allows detection of all fragments with 4π solid angle (using a smaller solid angle decreases the yield and may introduce some unwanted asymmetry effect). As the momenta gained in Coulomb explosion are very large (between 50 and 400 atomic units of momentum), electric fields used for CEI are usually higher than in other coincidence measurements. As the kinetic energy of the fragments is of the same order of magnitude (several eV) for different masses, protons have a large velocity due to their small mass and show thus a larger spatial spread; investigating fragmentation pathways without a single proton can thus be beneficial. Another possibility is to use electrostatic lenses to modify the imaging properties of the spectrometer.

When fragment ions have similar mass-to-charge ratios, their TOF distributions can overlap so that a certain hit on the detector cannot readily be assigned to a specific fragment. If all fragments from a Coulomb explosion are detected, this is not a problem as the correct assignment can be found by making use of momentum conservation (see section 4.6). This does not work, however, when neutral fragments are created in the break-up. As they cannot be detected, the sum momentum of the measured particles corresponds to the (negative) sum momentum of the undetected particle(s). For larger molecules, neutral hydrogen atoms are frequently emitted, carrying only little momentum. For this application, a setup has recently been designed that uses a high field (120 V cm^{-1}), together with an electrostatic lens and a drift region, to separate fragmentation pathways that differ in the amount of neutral hydrogen loss [97].

4.5. Detectors

Whatever the exact implementation of the spectrometer is: to extract three-dimensional momentum information for individual ions, both time and position information have to be recorded. The detectors thus need to fulfill the following requirements: single particle sensitivity, accurate time and position retrieval of the impact, and small dead-times to allow recording several particles from the molecular break-up.

The best answer to these prerequisites is currently given by a combination of a stack of microchannel plates (MCPs) and a position sensitive anode. Solid-state detectors such as complementary metal oxide semiconductor (CMOS) or charge-coupled device sensors do usually not fulfill the requirement of fast and accurate timing information due to their relatively long read-out times. In recent years, however, there has been significant progress in the development of CMOS pixel detectors for coincident detection, reaching now time-resolution of a few nanoseconds and position resolution of up to 1:300 [98–100]. In particular the small dead-time, allowing to detect many particle impacts within a few nanoseconds, is a promising aspect of this approach.

For the experiments described below, a commercially available detector from RoentDek [101], containing an MCP stack and a delay-line anode, was used. The MCP is used as an electron multiplier to extract a measurable signal from a single impinging particle (ions in the case of CEI). For that purpose, a voltage of roughly 1 kV is applied between front and back of the MCP, leading to an electron avalanche within its pores; to achieve a higher amplification, two (chevron configuration) or three (Z-stack) MCPs are mounted in series. The electron cloud emitted from the back of the MCP stack is then attracted by the anode which is set to higher positive voltage than the back of the MCP.

The delay line itself is essentially a helical wire; the position of the emitted electron cloud (and thus the initial impact position) is encoded in the propagation time of the signal to the two ends [33]. Two perpendicularly mounted delay lines allow one to determine the x- and y coordinate of the impact. In the case of multiple hits, the propagation time on the anode leads to dead-time effects and ambiguities in the position determination; it has proven beneficial to use three delay-lines in a hexagonal layout [102] to achieve dead-times below 20 ns and a spatial resolution up to roughly 1:800 (100 μm at 80 mm diameter).

To decouple the signals of the MCP and the delay-line anodes (usually pulses of a few mV) from the high voltage, a high-pass is used, complemented by potentiometers to optimize the signal shape. Each signal is then fed into an amplifier and a constant fraction discriminator (CFD). Contrary to commonly used leading-edge triggers, the CFD allows one to determine the timing information independent of the height of the pulse. This avoids jitter due to the different pulse heights that naturally occur from an MCP and allows one to achieve a timing resolution of roughly 200 ps. A more detailed description on the working principle of a CFD can be found in various manuals.

4.6. Data acquisition and analysis

The raw data of the experiment is essentially timing information: the time stamp of the pulsed photon beam, as well as the signals of the MCP and the delay-line anode for each ion are the ingredients to calculate impact position and TOF of the particles, which in turn are used to calculate momenta. The output signals of the CFD are recorded by a time-to-digital converter and then stored on a computer hard disk. Usually, the MCP pulse is used as a trigger and a time window is given that defines which hits on the detector belong to one ‘event’, i.e. to one molecular break-up. For the experiments described below, a cronologic HPTDC8 card was used, together with the data acquisition and analysis program COBOLD by RoentDek. Roughly 1 GB of raw data is produced per hour of measurement. The fact that all available information is stored for every molecular break-up separately allows one to ‘rerun’ the experiment offline as often as is needed to calibrate the experimental parameters.

In some applications, the signals of a delay-line anode are directly fed into an analog-to-digital converter, recording thus the pulse shape and allowing to separate two overlapping signals. In the case of CEI, the difference in the TOFs for different ions are usually large enough so that overlapping hits do not play a significant role.

The data analysis for the results shown below was performed with the C++-based framework ROOT [103] and consisted of essentially two steps that are common for all COLTRIMS experiments: first, the recorded time stamps have to be translated into position (x, y) and TOF information; second, the momentum vectors are calculated from the coordinates (x, y, TOF).

In the first step, the run-times of the signals are converted into position information, possible non-linearities of the detector are corrected and consistency checks for the signals of the three anode layers are performed. In the second step, the geometry of the setup and the electric field strength are used to calculate the momenta gained in the Coulomb explosion. Important parameters are: the length and the electric field strength of the spectrometer; the projected position of the interaction region on the detector (which is not

necessarily the detector center); the delay between the timing signal of the photon beam and the actual time of ionization; and the velocity of the molecular jet. Thanks to the possibility to 'rerun' the experiment in the analysis, the exact values of these parameters can be determined *a posteriori*. This is done by resorting to symmetry and conservation considerations: the kinetic energy that a fragment gained in the Coulomb explosion must be independent of its propagation direction; the sum momentum distribution of a molecular fragmentation must be centered at zero in the center-of-mass system etc. Especially the calibration of the spectrometer length(s) and the electric field strength(s) can be time-consuming. Due to the wealth of different break-up channels that occur in a Coulomb explosion measurement, such an experiment is in general 'self-calibrating', i.e. no additional calibration measurements are necessary. The fragment momenta thus obtained can be displayed in histograms and be used to investigate correlations and calculate further quantities.

In the case of chiral molecules, it is particularly important that the coordinate system in which the momenta are calculated corresponds to the detector orientation in the actual laboratory system—if one of the coordinate axes has the wrong sign, right-handed structures will appear left-handed.

5. Determining the handedness of single molecules: the example of CHBrClF

This section illustrates how the above considerations come to life in the investigation of the chiral prototype CHBrClF. Additional information can be found in previous publications [17, 18].

5.1. Preparing and performing the measurement

In order to demonstrate the separation of enantiomers, the chiral prototype CHBrClF was chosen (see figure 6). Both strong-field and single-photon ionization were used to induce the fragmentation. The strong-field experiment was performed at the Goethe-University Frankfurt (Germany) using a Titan-sapphire femtosecond laser (KMLabs Wyvern500) at 100 kHz repetition rate. For the single-photon case, the experiment was brought to the beamline SEXTANTS at the synchrotron radiation source SOLEIL (Gif-sur-Yvette, France). The photon energy in this case was 710 eV. For the results presented below, several grams of CHBrClF were obtained either via fluorination of $CHBr_2Cl$ with SbF_3 in presence of Br_2 [104] or by substituting one bromine of $CHBr_2Cl$ via HgF_2 [105]. As the equilibrium vapor pressure for CHBrClF at room temperature is around 600 mbar, a recipient with the liquid sample could be directly connected to the gas line leading to the nozzle (diameter 30 μm for the laser and 60 μm for the synchrotron experiment). The integral event rate (all ionization events) was between 10 and 20 kHz in both cases, the data acquisition time 11 h at the laser and 83 h at the synchrotron. Due to the fact that the fraction of five-particle fragmentation channels was 5×10^{-6} in the laser experiment and 7×10^{-5} for the synchrotron [18], a significantly higher amount of relevant break-ups was recorded in the latter case.

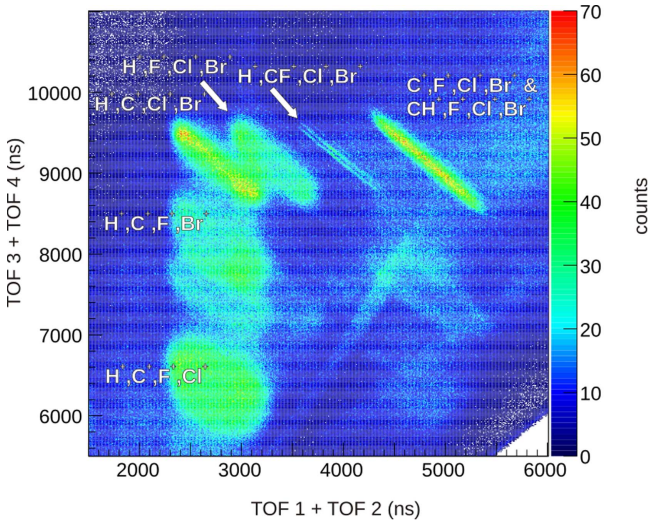

Figure 3. Four-particle coincidence spectrum of CHBrClF after single-photon ionization with $h\nu = 710$ eV. On the x-axis, the sum of time-of-flights for the first two ions is plotted, on the y-axis the sum of the third and fourth ion. When all fragments from a specific molecule are recorded, the events arrange on a line. As chlorine and bromine have different isotopes, several lines appear for different total masses of the CHBrClF isotopes. For incomplete fragmentation pathways, broader features can be identified. Figure reproduced from [18] John Wiley & Sons. © 2016 WILEY-VCH Verlag GmbH & Co. KGaA, Weinheim.

5.2. Identification of molecular break-ups

Multiple ionization and fragmentation of a molecule is a statistical process. As a result, every Coulomb explosion experiment yields a multitude of molecular break-up channels that are recorded simultaneously. A very convenient way to identify these break-ups are photoion coincidence spectra. In the basic form—the photoion–photoion-coincidence spectrum (PIPICO)—the TOF of the first and second hit on the detector TOF_1 and TOF_2 are plotted on the $x-$ and $y-$axis respectively. With the knowledge of the geometry and electric fields of the spectrometer, the mass-to-charge ratio of these hits can be identified as in conventional mass-spectrometry. A 'complete' fragmentation, i.e. a fragmentation for which the two fragment masses add up to the parent mass, is characterized by a narrow line in the PIPICO spectrum; in this case TOF_2 is a function of TOF_1 due to momentum conservation in the TOF direction. Broader features indicate a break-up where additional particle(s) carry away momentum. The momenta of the emitted electrons—and those of the exciting photons—can be neglected compared to the ion momenta gained in Coulomb explosion.

For multiple fragmentation, higher-order coincidence spectra can be created. Figure 3 shows the coincidence of four ions from the fragmentation of CHBrClF (single-photon excitation). The sum of the TOFs of the first two particles is plotted against the TOF sum of the third and fourth particle. Again, sharp features are visible if the fragments add up to the

mass of the parent molecule and thus fulfill momentum conservation (as in the case of {CF^+, H^+, Cl^+, Br^+}). The substructure originates from the different masses of the naturally occurring isotopes. If the recorded fragments do not add up to the total mass, broader features are visible. By setting time windows for the different detector hits, relevant fragmentation pathways can be selected for further analysis.

5.3. Calculation of momenta

The next step of the analysis is to calculate momenta for one or several of these selected pathways, using the equation (2). For CHBrClF, the fragmentation into five singly charged atomic ions was chosen for first analysis. As the narrow lines in the coincidence spectra indicate, the different isotopic channels could be separated and narrow windows on the total momentum in all three directions applied to reduce background.

It can occur, however, that fragments with similar mass-to-charge ratios have overlapping TOF distributions so that a certain hit cannot be unambiguously assigned to a mass-to-charge ratio. This is for example the case for the isotopically chiral species $CHBrCl_2$ (see [17] and supplementary material there). In that case, different permutations have to be tested. If one (and only one) combination yields a sum momentum close to zero, the assignment of masses is considered as correct. For two particles, this swapping can be implemented manually in the analysis code. A recursive algorithm that solves this ambiguity problem for an arbitrary number of particles has been described in [106].

5.4. Distinction of enantiomers

To determine the handedness of a molecular structure, a measurable quantity has to be found that is distinct for the two enantiomers, even though they are rotated randomly in space. A pseudoscalar, i.e. a scalar quantity that changes sign upon space inversion, is ideally suited for chiral molecules with one stereocenter. The triple product $\vec{A} \cdot (\vec{B} \times \vec{C})$ of the momentum vectors $\vec{A}$, $\vec{B}$ and $\vec{C}$ is the easiest example to construct a pseudoscalar for data obtained from Coulomb explosion. This means that three linearly independent momenta need to be measured. This a special case of the general rule that at least three linearly independent vectors are required to define a left- or right-handed object.

As discussed in the previous subsection, the fragmentation into five singly charged atomic ions was selected because the clearest signal of enantiomer separation was expected there. Only the isotopes ^{35}Cl and ^{79}Br were considered in the further analysis. A normalized triple product

$$\cos(\theta) = \frac{\vec{p}_F \cdot (\vec{p}_{Cl} \times \vec{p}_{Br})}{|\vec{p}_F| \cdot |\vec{p}_{Cl} \times \vec{p}_{Br}|} \qquad (3)$$

was calculated using the three heaviest fragments $^{79}Br^+$, $^{35}Cl^+$ and $^{19}F^+$. This quantity is referred to as $\cos(\theta)$ because it can be visualized by the angle between $\vec{p}_F$ and the normal vector of the plane spanned by $\vec{p}_{Cl}$ and $\vec{p}_{Br}$ (see inset in figure 4). The order in the triple product was chosen in a way that negative values correspond to an *S*-type configuration and positive values to an *R*-type configuration according to the CIP-rules [10, 11].

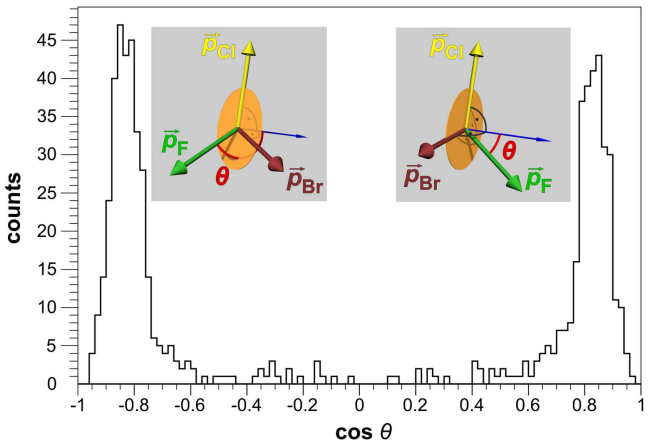

Figure 4. The chirality parameter $\cos(\theta)$ as defined in equation (3) after ionization of CHBrClF with femtosecond laser pulses. As is expected for a racemic mixture, the abundance for the two enantiomers is equal within the statistical uncertainty. The inset shows the graphical interpretation of $\cos(\theta)$. Figure reproduced from [17] with permission by AAAS.

Figure 4 shows the main result of the investigation, obtained by ionization with a femtosecond laser. Two distinct peaks are visible, equally populated within the statistical uncertainty (329 *S*- and 302 *R*-type structures) as expected from a racemic mixture. The fact that almost no background is present between them implies that for every single molecule detected in this break-up channel, the absolute configuration can be determined with a high degree of reliability. As figure 3 demonstrates, many break-up channels naturally occur after multiple ionization of the molecule. If these channels contain information on the absolute configuration, the statistical significance of the result can be increased tremendously because those channels have a much higher yield [18]. As an example, the separation of enantiomers for the channel {CH^+, F^+, Cl^+, Br^+} (with possible contaminations of the proton-missing channel {C^+, F^+, Cl^+, Br^+}) is shown in figure 5. The consistency of the assignment is checked by using different combinations of momentum vectors in analogy to equation (3) and plotting them in a two-dimensional histogram (which is obviously also possible for the complete fragmentation, not shown here). These results demonstrate that also molecular ions can be used to infer the molecular handedness, notwithstanding a higher fraction of ambiguous events (region around $\cos(\theta) = 0$).

Events with only three detected ions can be consulted as well when additional fragment(s) carry momentum so that three linearly independent momentum vectors exist. In this case, the amount of ambiguous events is so high that a determination on the single-molecule basis is hardly possible [18].

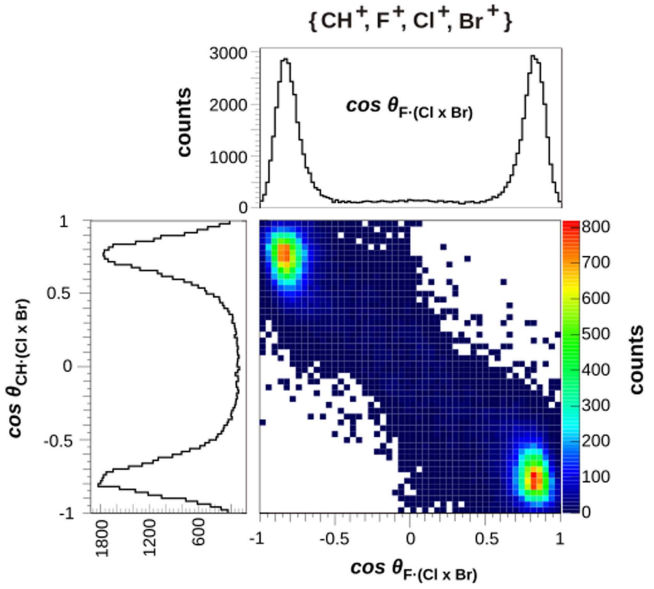

Figure 5. A two-dimensional plot of the chirality parameter for different fragment combinations in the break-up $\{CH^+, F^+, Cl^+, Br^+\}$ after single-photon ionization ($h\nu = 710$ eV). The location of the maxima on the negative diagonal indicates a consistent assignment of handedness. Figure reproduced from [18] John Wiley & Sons. © 2016 WILEY-VCH Verlag GmbH & Co. KGaA, Weinheim.

5.5. Visualization of momenta and comparison to initial structure

The most intuitive way to visualize the momentum vectors and to compare them to the molecular structure, is to plot them in a three-dimensional representation. As the molecules from the jet—and consequently the measured momenta—are rotated randomly in the laboratory space, the coordinate system for this representation has to be defined by the measured momenta themselves. Several physically reasonable possibilities exist for this transformation. In the case of CHBrClF, the following definitions for the unit vectors of the new coordinate system $\hat{x}'$, $\hat{y}'$ and $\hat{z}'$ turned out to yield an illustrative representation of the momenta:

$$\hat{x}' = \frac{\vec{p}_C}{|\vec{p}_C|}, \tag{4a}$$

$$\hat{y}' = \frac{\vec{p}_{Cl} + \vec{p}_{Br}}{|\vec{p}_{Cl} + \vec{p}_{Br}|}, \tag{4b}$$

$$\hat{z}' = \hat{x}' \times \hat{y}', \tag{4c}$$

where the momenta $\vec{p}_i$ are given in the center-of-mass system of the parent molecule in the laboratory space, i.e. in the frame of reference where the momentum sum is 0. In short, this means that one axis is defined by the carbon momentum, and a second axis by the sum of the heavy elements bromine and chlorine. The carbon has non-zero momentum after Coulomb explosion because it is only in the (approximate) geometrical center, not in the center-of-mass of the molecule. Figure 6 shows the transformed momenta, overlaid with a structure model of the molecule. The rotation is chosen in a way that the carbon momentum points away from the spectator and is thus barely visible.

The fact that the fragment momenta actually point in the bond direction was confirmed by a classical simulation. Point charges were assumed at the equilibrium positions obtained from [108]. These charges were propagated step-wise by integrating the classical equation of motion with purely Coulombic forces ($F \propto 1/r^2$). The angles between the momentum directions deviated only by a few degree from the bond angles, indicating that the axial recoil approximation still holds in this case. By multiplying the initial positions with random factors from a Gaussian distribution, the distribution of the chirality parameter could be reproduced well. The inverse problem, i.e. the retrieval of a structure from the measured data (no results shown), has been far less successful as reported previously for other molecules [46].

6. Perspectives

The results in the previous section can be considered as a proof-of-principle that the handedness of individual molecules can be determined by CEI. Which future directions are possible from this starting point? Without claiming completeness, three main lines of research will be sketched in the following: extension to larger molecules, coincident measurement of electron momenta together with Coulomb explosion, and the investigation of light-induced stereodynamics by pump–probe experiments.

6.1. Application to larger molecules

It should be obvious that CEI is not a very suitable technique for investigating complex molecules such as proteins. The preference for volatile compounds could, however, complement x-ray diffraction for the determination of absolute configuration. Additionally, the enantiomeric excess can in principle be determined very accurately since the precision for experiments with low background is mainly limited by the statistical error $\delta\epsilon/\epsilon$ due to the number N of molecules: $\delta\epsilon/\epsilon = 1/\sqrt{N}$.

A recent investigation of the chiral ethane derivative halothane ($CHClBrCF_3$) demonstrated that the handedness could also be determined for a more complex species [63]. The fragmentation into CH^+, Cl^+, Br^+ and CF_3^+ showed a clear signal for the two enantiomers, again from a racemic mixture.

As a rather large amount of sample is currently needed to perform CEI on neutral species (around 1 g, corresponding to 10 mMol), the substances investigated with COLTRIMS so far have only been available as a racemic mixture. To unambiguously prove that the technique can relate the macroscopic and the microscopic assignment of handedness, an experiment on an enantioenriched sample with known composition needs to be performed as in the case of foil-induced Coulomb explosion [19]. For larger species, enantiopure samples are commercially available. In the next years,

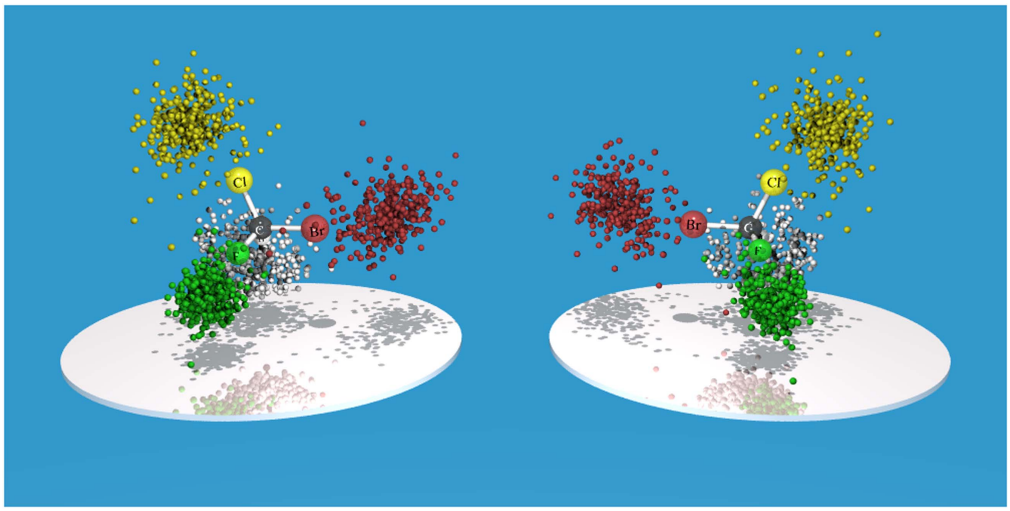

Figure 6. Three-dimensional representation of the linear momenta in the molecular frame for the fragmentation into five atomic ions (laser excitation). The momenta are rotated to overlay with a structure model. Color codes are white: H; black: C; green: F; yellow: Cl; red: Br. Reproduced from [107]. CC BY 3.0.

molecules such as propylene oxide, lactic acid or even the amino acid cysteine can possibly be investigated with CEI.

These molecules produce a large variety of fragmentation pathways, decreasing the probability of pathways that are significant for the determination of absolute configuration. In the case of coincidence detection, this requires higher detection rates or longer measurement times. Non-coincident methods to determine absolute configuration from Coulomb explosion such as in [52] are thus another promising approach for more complex species.

A general impediment for the CEI approach is that for complex molecules, the axial recoil approximation is expected to break down and intermediate structures that do not conserve the configuration may occur during the break-up. If the determination of configuration is possible at all in those cases, it will need a better modeling of the fragmentation process and a more sophisticated analysis.

6.2. Coincident measurement of electrons and ions

A prominent aspect in the investigation of chiral molecules is the asymmetric interaction with circularly polarized light (see section 1). Although several groups report differences in the ion yield after irradiation with nanosecond [15] or femtosecond laser pulses [109], no significant difference in the number of left- and right-handed molecules has so far been identified after Coulomb explosion of CHBrClF and halothane.

In the last 15 years, large asymmetry effects have been found in the angular emission of photoelectrons from randomly oriented chiral molecules. The so-called PECD [110] has been observed with single-photon [11] and multi-photon ionization [12]. As the COLTRIMS technique can detect both ion and electron momenta in coincidence, the electron emission direction can be plotted in the molecular frame. The main problem with this approach is currently the large number of electrons (at least four) that must be removed to determine the absolute configuration. The variety of ionization and charge rearrangement processes leads to a broad distribution of detected electrons that has so far concealed a clear photoelectron signal. For double ionization of propylene oxide (also known as methyl oxirane), one molecular axis could be defined and an enhancement of PECD for certain molecular orientations be reported [97].

6.3. Light-induced stereodynamics

Many molecules exist that change their configuration upon photo-excitation, i.e. that have a different structure in excited electronic states than they have in the ground state. Many proposals exist to use this effect for chiroptical switches (a remarkable implementation being [111]), for optical enantiopurification [112, 113] and to investigate fundamental questions like the tunneling between the left- and right-handed state [114] or the parity violation in chiral molecules [115, 116]. By inducing the transformation with a pump pulse and probing the structure by CEI, information on the structural changes could be retrieved. First experiments have been performed on formic acid (HCOOH) that is planar in the ground state and chiral in the $\pi^\star$ state [117]. The tunnel barrier between left- and right-handed state is expected to be much lower than for molecules that are chiral in the ground state, allowing oscillations between these two states in an experimentally accessible time-scale [116]. It should, however, be noted that CEI cannot distinguish a racemic mixture from a quantum-mechanical superposition of left- and right-handed molecular state (see [118] for a proposal to do so) so that for the observation of tunneling, an asymmetric state has to be prepared in the pump step.

7. Summary

This tutorial describes how coincident momentum imaging allows one to determine the stereochemical configuration of individual molecules. Molecular species that are multiply ionized within a few femtoseconds undergo Coulomb explosion; the momentum vectors of the cations produced in this explosion retain information on the initial molecular structure. Coincident measurement of these momenta allows one to retrieve structural features for single molecules and opens the possibility to explore various correlations between the fragments.

First experiments to determine molecular structure in this way date back to the 1970s. In the last 20 years, progress in femtosecond lasers and synchrotron sources, as well as in detector technology has paved the way to apply CEI to larger molecules with chemical interest. Experiments described here and in previous papers have demonstrated that individual right- and left-handed molecular structures can be distinguished.

Main technical challenges on the way to a routine analysis are the relatively large amount of sample needed, the long measurement time (several hours) and the data analysis procedure that has not been automatized so far. On a fundamental level, it is still unclear up to which size of the molecule ion momenta can reliably reveal structure. But CEI of chiral molecules offers more than the analysis of equilibrium structure: it allows one to take detailed pictures of the light–matter interaction of individual chiral molecules, i.e. by additionally measuring the emitted electrons' momenta or by employing pump–probe schemes.

Acknowledgments

The results upon which this tutorial is based are the work of numerous people. First and foremost, I would like to thank the atomic physics group at the Goethe-University in Frankfurt (Germany), in particular Reinhard Dörner, Markus Schöffler, Horst Schmidt-Böcking, Till Jahnke, Maksim Kunitski and Lothar Schmidt for sharing their expertise and their enthusiasm.

Robert Berger, Sebastian Marquardt and Sabrina Marquardt (now at Philipps-University Marburg, Germany) have always been inspiring and insightful partners for discussion. A special thanks is due to Julia Kiedrowski, Alexander Schießer and Michael Reggelin at TU Darmstadt (Germany), as well as to Michael Mazenauer, Benjamin Spenger and Jürgen Stohner at the Zurich University of Applied Sciences (Wädenswil, Switzerland) for preparing the samples.

Parts of the work were performed at Synchrotron SOLEIL (Gif-sur-Yvette, France) where we enjoyed funding and outstanding support, in particular from Nicolas Jaouen at the beamline SEXTANTS. This work was supported by the State Initiative for the Development of Scientific and Economic Excellence (LOEWE) in the LOEWE-Focus ELCH (Electron Dynamics of Chiral Systems). I thank the University of Kassel for granting me an independent junior researcher position that gave me the freedom to elaborate this tutorial.

ORCID

Martin Pitzer https://orcid.org/0000-0002-6151-182X

References

[1] van't Hoff J H 1874 Sur les formules de structure dans l'espace *Archives Néerlandaises des Sciences Exactes et Naturelles* **9** 445–54
[2] Le Bel J-A 1874 Sur les relations qui existent entre les formules atomiques des corps organiques et le pouvoir rotatoire de leurs dissolutions *Bull. Soc. Chim. Paris* **T 22** 337–47
[3] Kelvin L 1894 *The Molecular Tactics of a Crystal* (Oxford : Oxford University Press)
[4] Moss G P 1996 Basic terminology of stereochemistry (IUPAC Recommendations 1996) *Pure Appl. Chem.* **68** 2193–222
[5] Wolf C 2007 *Dynamic Stereochemistry of Chiral Compounds : Principles and Applications* 1st edn (Cambridge: Royal Society of Chemistry)
[6] Berova N, Polaravapu P L, Nakanishi K and Woody R W (ed) 2012 *Comprehensive Chiroptical Spectroscopy* (Hoboken, NJ: Wiley)
[7] Fischer E 1891 Ueber die Configuration des Traubenzuckers und seiner Isomeren *Ber. Dtsch. Chemischen Ges.* **24** 1836–45
[8] Bijvoet J M, Peerdeman A F and van Bommel A J 1951 Determination of the absolute configuration of optically active compounds by means of x-rays *Nature* **168** 271–2
[9] Cahn R S and Ingold C K 1951 Specification of configuration about quadricovalent asymmetric atoms *J. Chem. Soc.* **1951** 612–22
[10] Cahn R S, Ingold C K and Prelog V 1966 Specification of molecular chirality *Angew. Chem., Int. Ed. Engl.* **5** 385–415
[11] Böwering N, Lischke T, Schmidtke B, Müller N, Khalil T and Heinzmann U 2001 Asymmetry in photoelectron emission from chiral molecules induced by circularly polarized light *Phys. Rev. Lett.* **86** 1187–90
[12] Lux C, Wollenhaupt M, Bolze T, Liang Q, Köhler J, Sarpe C and Baumert T 2012 Circular dichroism in the photoelectron angular distributions of camphor and fenchone from multiphoton ionization with femtosecond laser pulses *Angew. Chem., Int. Ed. Engl.* **51** 5001–5
[13] Janssen M H M and Powis I 2014 Detecting chirality in molecules by imaging photoelectron circular dichroism *Phys. Chem. Chem. Phys.* **16** 856–71
[14] Li R, Sullivan R, Al-Basheer W, Pagni R M and Compton R N 2006 Linear and nonlinear circular dichroism of R-(+)-3-methylcyclopentanone *J. Chem. Phys.* **125** 144304
[15] Bornschlegl A, Logé C and Boesl U 2007 Investigation of CD effects in the multi photon ionisation of R-(+)-3-methylcyclopentanone *Chem. Phys. Lett.* **447** 187–191
[16] Patterson M, Schnell M and Doyle J M 2013 Enantiomer-specific detection of chiral molecules via microwave spectroscopy *Nature* **497** 475–8
[17] Pitzer M *et al* 2013 Direct determination of absolute molecular stereochemistry in gas phase by Coulomb explosion imaging *Science* **341** 1096–100

[18] Pitzer M *et al* 2016 Absolute configuration from different multifragmentation pathways in light-induced Coulomb explosion imaging *ChemPhysChem* **17** 2465–72

[19] Herwig P *et al* 2013 Imaging the absolute configuration of a chiral epoxide in the gas phase *Science* **342** 1084–6

[20] Herwig P *et al* 2014 Absolute configuration assignment of a chiral molecule in the gas phase using foil-induced Coulomb explosion imaging *Phys. Rev.* A **90** 052503

[21] Vager Z, Gemmell D S and Zabransky B J 1976 Dissociation of fast HeH^+ ions traversing thin foils *Phys. Rev.* A **14** 638–41

[22] Chandler D W and P L Houston 1986 MUPPATSa multiparticle 3D imaging detector system *Nucl. Instrum. Methods Phys. Res.* B **13** 673–7

[23] Kella D *et al* 1993 A system for Coulomb explosion imaging of small molecules at the weizmann institute *Nucl. Instrum. Methods Phys. Res.* A **329** 440–52

[24] Vager Z, Kanter E P, Both G, Cooney P J, Faibis A, Koenig W, Zabransky B J and Zajfman D 1986 Direct determination of the stereochemical structure of CH_4^+ *Phys. Rev. Lett.* **57** 2793–5

[25] Vager Z, Naaman R and Kanter E P 1989 Coulomb explosion imaging of small molecules *Science* **244** 426–31

[26] Faibis A, Kanter E P, Tack L M, Bakke E and Zabransky B J 1987 Geometrical structure of carbon ion (C3+) *J. Phys. Chem.* **91** 6445–7

[27] Feldman H, Kella D, Malkin E, Miklazky E, Vager Z, Zajfman J and Naaman R 1990 The structure of carbon clusters as studied by the Coulomb explosion method *J. Chem. Soc. Faraday Trans.* **86** 2469–72

[28] Zajfman D, Belkacem A, Graber T, Kanter E P, Mitchell R E, Naaman R, Vager Z and Zabransky B J 1991 Measurement of the distribution of bond angles in H_2O^+ *J. Chem. Phys.* **94** 2543–7

[29] de Brujin D P and Los J 1982 Time and position-sensitive detector for dissociative processes in fast beams *Rev. Sci. Instrum.* **53** 1020–6

[30] Chandler D W and Houston P L 1987 Two-dimensional imaging of state-selected photodissociation products detected by multiphoton ionization *J. Chem. Phys.* **87** 1445–7

[31] Werner U, Beckord K, Becker J and Lutz H O 1995 3D imaging of the collision-induced Coulomb fragmentation of water molecules *Phys. Rev. Lett.* **74** 1962–5

[32] Becker J, Beckord K, Werner U and Lutz H O 1994 A system for correlated fragment detection in dissociation experiments *Nucl. Instrum. Methods Phys. Res.* A **337** 409–15

[33] Sobottka S E and Williams M B 1988 Delay-line readout of microchannel plates *IEEE Trans. Nucl. Sci.* **35** 348–51

[34] Eland J H D 1994 Simple two-dimensional position sensitive detector with short dead-time for coincidence experiments *Meas. Sci. Technol.* **5** 1501

[35] Hsieh S and Eland J H D 1997 Reaction dynamics of three-body dissociations in triatomic molecules from single-photon double ionization studied by a time- and position-sensitive coincidence method *J. Phys. B: At. Mol. Opt. Phys.* **30** 4515–34

[36] Frasinski L J, Codling K and Hatherly P A 1989 Covariance mapping: a correlation method applied to multiphoton multiple ionization *Science* **246** 1029–31

[37] Cornaggia C, Schmidt M and Normand D 1995 Laser-induced nuclear motions in the Coulomb explosion of $C_2H_2^+$ ions *Phys. Rev.* A **51** 1431–7

[38] Eppink A T J B and Parker D H 1997 Velocity map imaging of ions and electrons using electrostatic lenses: application in photoelectron and photofragment ion imaging of molecular oxygen *Rev. Sci. Instrum.* **68** 3477–84

[39] Stapelfeldt H, Constant E and Corkum P B 1995 Wave packet structure and dynamics measured by Coulomb explosion *Phys. Rev. Lett.* **74** 3780–3

[40] Légaré F, Lee K F, Litvinyuk I V, Dooley P W, Bandrauk A D, Villeneuve D M and Corkum P B 2005 Imaging the time-dependent structure of a molecule as it undergoes dynamics *Phys. Rev.* A **72** 052717

[41] Dörner R, Mergel V, Jagutzki O, Spielberger L, Ullrich J, Moshammer R and Schmidt-Böcking H 2000 Cold target recoil ion momentum spectroscopy: a 'momentum microscope' to view atomic collision dynamics *Phys. Rep.* **330** 95–192

[42] Ullrich J, Moshammer R, Dorn A, Dörner R, Schmidt L P H and Schmidt-Böcking H 2003 Recoil-ion and electron momentum spectroscopy: reaction-microscopes *Rep. Prog. Phys.* **66** 1463–545

[43] Jahnke T *et al* 2002 Circular dichroism in K-shell ionization from fixed-in-space CO and N_2 molecules *Phys. Rev. Lett.* **88** 73002

[44] Williams J B *et al* 2012 Imaging polyatomic molecules in three dimensions using molecular frame photoelectron angular distributions *Phys. Rev. Lett.* **108** 233002

[45] Kitamura T, Nishide T, Shiromaru H, Achiba Y and Kobayashi N 2001 Direct observation of 'dynamic' chirality by Coulomb explosion imaging *J. Chem. Phys.* **115** 5–6

[46] Gagnon J, Lee K F, Rayner D M, Corkum P B and Bhardwaj V R 2008 Coincidence imaging of polyatomic molecules via laser-induced Coulomb explosion *J. Phys. B: At. Mol. Opt. Phys.* **41** 215104

[47] Matsuda A, Fushitani M, Thomas R D, Zhaunerchyk V and Hishikawa A 2009 Multiple explosion pathways of the deuterated benzene trication in 9 fs intense laser fields *J. Phys. Chem.* A **113** 2254–60

[48] Rajgara F A, Krishnamurthy M, Mathur D, Nishide T, Shiromaru H and Kobayashi N 2004 Coulombic and non-Coulombic fragmentation of highly charged benzene *J. Phys. B: At. Mol. Opt. Phys.* **37** 1699

[49] Wang E, Shan X, Shen Z, Li X, Gong M, Tang Y and Chen X 2015 Three-body-fragmentation dynamics of CO_2^{4+} investigated by electron collisions at an impact energy of 500 eV *Phys. Rev.* A **92** 062713

[50] Singh R, Bhatt P, Yadav N and Shanker R 2013 Kinematics and dissociation dynamics of a water molecule under the impact of 10 keV electrons *J. Phys. B: At. Mol. Opt. Phys.* **46** 085203

[51] Zawatzky K *et al* 2014 Coulomb explosion imaged cryptochiral (R, R)-2,3dideuterooxirane: unambiguous access to the absolute configuration of (+)- glyceraldehyde *Chem. Eur. J.* **20** 5555–8

[52] Christensen L, Nielsen J H, Slater C S, Lauer A, Brouard M and Stapelfeldt H 2015 Using laser-induced Coulomb explosion of aligned chiral molecules to determine their absolute configuration *Phys. Rev.* A **92** 033411

[53] Sakurai J J 1994 *Modern Quantum Mechanics* (Reading, MA: Addison-Wesley)

[54] Yeh J J and Lindau I 1985 Atomic subshell photoionization cross sections and asymmetry parameters: $1 \leqslant Z \leqslant 103$ *At. Data Nucl. Data Tables* **232** 1–155

[55] Carlson T A, Hunt W E and Krause M O 1966 Relative abundances of ions formed as the result of inner-shell vacancies in atoms *Phys. Rev.* **151** 41–7

[56] Brünken S, Gerth C, Kanngießer B, Luhmann T, Richter M and Zimmermann P 2002 Decay of the Ar $2s^{-1}$ and $2p^{-1}$ and Kr $3p^{-1}$ and $3d^{-1}$ hole states studied by photoelectron-ion coincidence spectroscopy *Phys. Rev.* A **65** 042708

[57] Kučas S, Karazija R and Momkauskaitė A 2012 Cascades after K-vacancy production in atoms and ions of light elements *Astrophys. J.* **750** 90

[58] Knapp A *et al* 2002 *Phys. Rev. Lett.* **89** 033004

[59] Eland J H D, Tashiro M, Linusson P, Ehara M, Ueda K and Feifel R 2010 Double core hole creation and subsequent auger decay in NH_3 and CH_4 molecules *Phys. Rev. Lett.* **105** 213005

[60] Morin P and Nenner I 1986 Atomic autoionization following very fast dissociation of core-excited HBr *Phys. Rev. Lett.* **56** 1913–6

[61] Roithová J, Žabka J, Herman Z, Thissen R, Schröder D and Schwarz H 2006 Reactivity of the $CHBr^{2+}$ dication toward molecular hydrogen *J. Phys. Chem.* A **110** 6447–53

[62] Erk B *et al* 2014 Imaging charge transfer in iodomethane upon x-ray photoabsorption *Science* **345** 288–91

[63] Pitzer M *et al* 2016 Stereochemical configuration and selective excitation of the chiral molecule halothane *J. Phys. B: At. Mol. Opt. Phys.* **49** 234001

[64] Nagaoka S *et al* 2011 A study to control chemical reactions using Si:2p core ionization: site-specific fragmentation *J. Phys. Chem.* A **115** 8822–31

[65] Ammosov M V, Delone N B and Krainov V P 1986 Tunnelionization of complex atoms and of atomic ions in an alternating electromagnetic field *Sov. Phys.-JETP* **64** 1191–4

[66] Tong X M, Zhao Z X and Lin C D 2002 Theory of molecular tunneling ionization *Phys. Rev.* A **66** 033402

[67] Kjeldsen T K, Bisgaard C Z, Madsen L B and Stapelfeldt H 2005 Influence of molecular symmetry on strong-field ionization: studies on ethylene, benzene, fluorobenzene, and chlorofluorobenzene *Phys. Rev.* A **71** 013418

[68] Brabec T, Côté M, Boulanger P and Ramunno L 2005 Theory of tunnel ionization in complex systems *Phys. Rev. Lett.* **95** 073001

[69] Keldysh L V 1965 Ionization in the field of a strong electromagnetic wave *Sov. Phys.-JETP* **5** 1307–14

[70] Faisal F H M 1973 Multiple absorption of laser photons by atoms *J. Phys. B: At. Mol. Phys.* **6** L89–92

[71] Reiss H R 1980 Effect of an intense electromagnetic field on a weakly bound system *Phys. Rev.* A **22** 1786–813

[72] Ivanov M Y, Spanner M and Smirnova O 2005 Anatomy of strong field ionization *J. Mod. Opt.* **52** 165–84

[73] Becker A and Faisal F H M 2005 Intense-field many-body S-matrix theory *J. Phys. B: At. Mol. Opt. Phys.* **38** R1–56

[74] Muth-Böhm J, Becker A and Faisal F H M 2000 Suppressed molecular ionization for a class of diatomics in intense femtosecond laser fields *Phys. Rev. Lett.* **85** 2280–3

[75] Becker W, Liu X J, Ho P J and Eberly J H 2012 Theories of photoelectron correlation in laser-driven multiple atomic ionization *Rev. Mod. Phys.* **84** 1011–41

[76] Corkum P B 1993 Plasma perspective on strong field multiphoton ionization *Phys. Rev. Lett.* **71** 1994–7

[77] Bhardwaj V, Rayner D, Villeneuve D and Corkum P 2001 Quantum interference in double ionization and fragmentation of C_6H_6 in intense laser fields *Phys. Rev. Lett.* **87** 253003

[78] Zuo T and Bandrauk A D 1995 Charge-resonance enhanced ionization of diatomic molecular-ions by intense lasers *Phys. Rev.* A **52** R2511–4

[79] Cornaggia C 2016 Electronic dynamics of charge resonance enhanced ionization probed by laser-induced alignment in C_2H_2 *J. Phys. B: At. Mol. Opt. Phys.* **49** 19LT01

[80] Zhao A, Sándor P, Tagliamonti V, Matsika S and Weinacht T 2016 Molecular double ionization using strong field few-cycle laser pulses *J. Phys. Chem.* A **120** 3233–40

[81] Pitzer M, Kunitski M, Jahnke T, Schmidt L P H, Schmidt-Böcking H, Dörner R and Schöffler M 2017 Coulomb explosion imaging as a tool to distinguish between stereoisomers *J. Vis. Exp.* accepted (https://doi.org/10.3791/56062)

[82] Rullière C (ed) 2005 *Femtosecond Laser Pulses* 2 edn (Berlin: Springer)

[83] Zhang X, Schneider E, Taft G, Kapteyn H, Murnane M and Backus S 2012 Multi-microjoule, MHz repetition rate Ti: sapphire ultrafast regenerative amplifier system *Opt. Express* **20** 7015–21

[84] Schriever C, Lochbrunner S, Krok P and Riedle E 2008 Tunable pulses from below 300 to 970 nm with durations down to 14 fs based on a 2 MHz ytterbium-doped fiber system *Opt. Lett.* **33** 192–4

[85] Rothhardt J, Haedrich S, Carstens H, Herrick N, Demmler S, Limpert J and Tuennermann A 2011 1 MHz repetition rate hollow fiber pulse compression to sub-100-fs duration at 100 W average power *Opt. Lett.* **36** 4605–7

[86] Puppin M, Deng Y, Prochnow O, Ahrens J, Binhammer T, Morgner U, Krenz M, Wolf R and Ernstorfer M 2015 500 kHz OPCPA delivering tunable sub-20 fs pulses with 15 W average power based on an all-ytterbium laser *Opt. Express* **23** 1491–7

[87] Brons J, Pervak V, Bauer D, Sutter D, Pronin O and Krausz F 2016 Powerful 100 fs scale Kerr-lens mode-locked thin-disk oscillator *Opt. Lett.* **41** 3567–70

[88] Gagnon E, Ranitovic P, Tong X M, Cocke C L, Murnane M M, Kapteyn H C and Sandhu A S 2007 Soft x-ray-driven femtosecond molecular dynamics *Science* **317** 1374–8

[89] Rothhardt J *et al* 2016 High-repetition-rate and high-photon-flux 70 ev high-harmonic source for coincidence ion imaging of gas-phase molecules *Opt. Express* **24** 18133–47

[90] Eland J H D 1987 The dynamics of three-body dissociations of dications studied by the triple coincidence technique PEPIPICO *Mol. Phys.* **61** 725–45

[91] Simon M, LeBrun T, Morin P, Lavollée M and Maréchal J L 1991 A photoelectron-ion multiple coincidence technique applied to core ionization of molecules *Nucl. Instrum. Methods Phys. Res.* B **62** 174

[92] Garcia G A, Cunha de Miranda B K, Tia M, Daly S and Nahon L 2013 DELICIOUS III: a multipurpose double imaging particle coincidence spectrometer for gas phase vacuum ultraviolet photodynamics studies *Rev. Sci. Instrum.* **84** 053112

[93] Ueda K and Eland J H D 2005 Molecular photodissociation studied by vuv and soft x-ray radiation *J. Phys. B: At. Mol. Opt. Phys.* **38** S839–59

[94] Calvert C R *et al* 2012 Liad-fs scheme for studies of ultrafast laser interactions with gas phase biomolecules *Phys. Chem. Chem. Phys.* **14** 6289–97

[95] Gaie-Levrel F, Garcia G A, Schwell M and Nahon L 2011 VUV state-selected photoionization of thermally-desorbed biomolecules by coupling an aerosol source to an imaging photoelectron/photoion coincidence spectrometer: case of the amino acids tryptophan and phenylalanine *Phys. Chem. Chem. Phys.* **13** 7024–36

[96] Miller D R 1988 Free jet sources *Atomic and Molecular Beam Methods* ed G Scoles (Oxford: Oxford University Press) pp 14–53

[97] Tia M *et al* 2016 Observation of enhanced chiral asymmetries in the inner-shell photoionization of uniaxially oriented methyloxirane enantiomers *J. Phys. Chem. Lett.* **8** 2780–6

[98] Amini K, Blake S, Brouard M, Burt M B, Halford E, Lauer A, Slater C S, Lee J W L and Vallance C 2015 Three-dimensional imaging of carbonyl sulfide and ethyl iodide photodissociation using the pixel imaging mass spectrometry camera *Rev. Sci. Instrum.* **86** 103113

[99] Vallance C *et al* 2014 Fast sensors for time-of-flight imaging applications *Phys. Chem. Chem. Phys.* **16** 383–95

[100] Jungmann J H, Gijsbertsen A, Visser J, Visschers J, Heeren R M A and Vrakking M J J 2010 A new imaging method for understanding chemical dynamics: efficient slice imaging using an in-vacuum pixel detector *Rev. Sci. Instrum.* **81** 103112

[101] http://roentdek.com
[102] Jagutzki O *et al* 2002 Multiple hit readout of a microchannel plate detector with a three-layer delay-line anode *IEEE Trans. Nucl. Sci.* **49** 2477–83
[103] https://root.cern.ch
[104] Swarts F 1893 Sur le fluorchlorbromméthane *Bull. Cl. Sci. Acad. R. Belg.* **26** 102–6
[105] Hine J, Dowell A M and Singley J E 1956 Carbon dihalides as intermediates in the basic hydrolysis of haloforms: IV. Relative reactivities of haloforms *J. Am. Chem. Soc.* **78** 479–82
[106] Wales B, Bisson E, Karimi R, Kieffer J-C, Légaré F and Sanderson J 2012 A coincidence detection algorithm for improving detection rates in Coulomb explosion imaging *Nucl. Instrum. Methods Phys. Res.* A **667** 11–5
[107] Pitzer M 2015 Koinzidenzmessungen an chiralen Molekülen: Absolutkonfiguration und Zirkulardichroismus *PhD Thesis* Goethe-Universität Frankfurt (http://publikationen.ub.uni-frankfurt.de/frontdoor/index/index/docId/37694)
[108] Jacob E J 1978 Structure of bromochlorofluoromethane by electron diffraction *J. Mol. Struct.* **52** 63–9
[109] Horsch P, Urbasch G, Weitzel K-M and Kröner D 2011 Circular dichroism in ion yields employing femtosecond laser ionizationthe role of laser pulse duration *Phys. Chem. Chem. Phys.* **13** 2378–86
[110] Ritchie B 1976 Theory of the angular distribution of photoelectrons ejected from optically active molecules and molecular negative ions *Phys. Rev.* A **13** 1411–5
[111] van Delden R A, ter Wiel M K J and Feringa B L 2004 A chiroptical molecular switch with perfect stereocontrol *Chem. Commun.* **2004** 200–1
[112] Salam A and Meath W J 1997 On the control of excited state relative populations of enantiomers using circularly polarized pulses of varying durations *J. Chem. Phys.* **106** 7865–8
[113] Fujimura Y, González L, Hoki K, Manz J and Ohtsuki Y 1999 Selective preparation of enantiomers by laser pulses: quantum model simulation for H_2POSH *Chem. Phys. Lett.* **306** 1–8
[114] Hund F 1927 Zur Deutung der Molekelspektren: III. Bemerkungen über das Schwingungs- und Rotationsspektrum bei Molekeln mit mehr als zwei Kernen *Zeitschrift für Physik* **43** 805–26
[115] Harris R A and Stodolsky L 1978 Quantum beats in optical activity and weak interactions *Phys. Lett.* B **78** 313–7
[116] Berger R 2003 Molecular parity violation in electronically excited states *Phys. Chem. Chem. Phys.* **5** 12–7
[117] Ng T L and Bell S 1974 The $\pi^* \leftarrow n$ transition of formic acid *J. Mol. Spectrosc.* **50** 166–81
[118] Cina J A and Harris R A 1995 Superpositions of handed wave functions *Science* **267** 832–3